

2012

Cell Permeabilization and Inhibition of Voltage-Gated Ca^{2+} and Na^{+} Channel Currents by Nanosecond Pulsed Electric Fields


Vasyl Nesin
Old Dominion University

Angela M. Bowman
Old Dominion University

Shu Xiao
Old Dominion University, sxiao@odu.edu

Andrei G. Pakhomov
Old Dominion University, apakhomo@odu.edu

Follow this and additional works at: https://digitalcommons.odu.edu/bioelectrics_pubs

 Part of the [Biomedical Engineering and Bioengineering Commons](#), [Biophysics Commons](#), and the [Nanoscience and Nanotechnology Commons](#)

Repository Citation

Nesin, Vasyl; Bowman, Angela M.; Xiao, Shu; and Pakhomov, Andrei G., "Cell Permeabilization and Inhibition of Voltage-Gated Ca^{2+} and Na^{+} Channel Currents by Nanosecond Pulsed Electric Fields" (2012). *Bioelectrics Publications*. 173.
https://digitalcommons.odu.edu/bioelectrics_pubs/173

Original Publication Citation

Nesin, V., Bowman, A. M., Xiao, S., & Pakhomov, A. G. (2012). Cell permeabilization and inhibition of voltage-gated Ca^{2+} and Na^{+} channel currents by nanosecond pulsed electric field. *Bioelectromagnetics*, 33(5), 394-404. doi:10.1002/bem.21696

Published in final edited form as:

Bioelectromagnetics. 2012 July ; 33(5): 394–404. doi:10.1002/bem.21696.

Cell permeabilization and inhibition of voltage-gated Ca^{2+} and Na^{+} channel currents by nanosecond pulsed electric fields

Vasyl Nesin¹, Angela M. Bowman¹, Shu Xiao^{1,2}, and Andrei G. Pakhomov^{1,*}

¹Frank Reidy Research Center for Bioelectrics, Old Dominion University, Norfolk, VA, USA.

²Dept. of Electrical and Computer Engineering, Old Dominion University, Norfolk, VA, USA.

Abstract

Previous studies have found that nanosecond pulsed electric field (nsPEF) exposure causes long-term permeabilization of the cell plasma membrane. In this study, we utilized the whole-cell patch-clamp method to study the nsPEF effect on currents of voltage-gated (VG) Ca^{2+} and Na^{+} channels (I_{Ca} and I_{Na} , respectively) in cultured GH3 and NG108 cells. We found that a single 300 or 600 ns pulse at or above 1.5–2 kV/cm caused prolonged inhibition of I_{Ca} and I_{Na} . Concurrently, nsPEF increased non-inactivating “leak” currents (I_{leak}), presumably due to the formation of nanoelectropores or larger pores in the plasma membrane. The nsPEF effects were similar in cells that were exposed intact and subsequently brought into the whole-cell recording configuration, and in cells that were first brought into the whole-cell configuration and then exposed. Although both I_{leak} and the inhibition of VG currents were enhanced at higher E-field levels, these two nsPEF effects showed relatively weak correlation with each other. In some cells, I_{leak} increased 10-fold or more while VG currents remained unchanged. At longer time intervals after exposure (5–15 min), I_{Ca} and I_{Na} could remain inhibited although I_{leak} had largely recovered. The causal relation of nsPEF inhibitory effects on VG currents and permeabilization of the plasma membrane is discussed.

Keywords

electropermeabilization; cell membrane; Ca channels; Na channels; patch clamp

INTRODUCTION

Electropermeabilization of the cell plasma membrane by high-voltage electric shocks is a well-established technique with multiple applications in science, medicine, and biotechnology [Neumann et al., 1989; Zimmermann and Neil, 1996; Teissie et al., 1999; Weaver, 2000; Pakhomov et al., 2010; Rubinsky, 2010]. The most widely, albeit not universally accepted mechanism underlying permeabilization is the formation of membrane pores, or electroporation. The size, density, and lifetime of electropores vary widely, depending on the electric pulse parameters, cell type, temperature, and other conditions. Compromising the plasma membrane barrier function by electroporation has multiple physiological consequences, including the loss of membrane potential; loss of intracellular solutes and uptake of extracellular solutes; colloid-osmotic imbalance, cell swelling and blebbing; and necrotic or apoptotic cell death.

*Correspondence to: Andrei G. Pakhomov, 4211 Monarch Way, Suite 300 Norfolk, VA 23508, USA, Phone: 210-204-9012, 757-683-8003; Fax: 757-451-101, andrei@pakhomov.net, apakhomo@odu.edu.

Most studies of conventional electroporation employed electric pulses of micro- to millisecond durations. Shorter pulses of higher intensity, which are also commonly referred to as nanosecond pulsed electric fields (nsPEF), were introduced in biological research as a means of bypassing the cell membrane and evoking intracellular effects [Schoenbach et al., 2001, 2007]. Although a number of studies were in agreement with this prediction [Beebe et al., 2003a, b; Deng et al., 2003; White et al., 2004], other investigations using more sensitive assays have established that the plasma membrane is not “exempt” from poration by nsPEF [Vernier et al., 2004, 2006; Pakhomov et al., 2007a, b, 2009; Napotnik et al., 2010]. As of today, the opening of small but stable membrane pores (“nanopores”) by nsPEF has been shown using the patch-clamp technique, by uptake of fluorescent dyes and reporter ions, by water uptake and colloid-osmotic changes in the cell volume, and by fast externalization of phosphatidylserine [Vernier et al., 2004, 2006; Pakhomov and Pakhomova, 2010]. The thresholds for nanopore formation were about 6 kV/cm for a single 60 ns pulse and 1 kV/cm for a 600 ns pulse [Ibey et al., 2009; Bowman et al., 2010], which is at or below the threshold for other reported nsPEF effects [Beebe et al., 2003a, b; White et al., 2004; Napotnik et al., 2010; Ren and Beebe, 2011]. Notably, increasing the nsPEF intensity or pulse number has led to opening of larger pores akin to conventional electroporation.

Although the finding of nanopore formation does not negate the possibility of direct intracellular effects of nsPEF, it has yet to be demonstrated if any intracellular effects can occur at field levels below the threshold for plasma membrane nanoporation [Napotnik et al., 2010]. Indeed, the conditions for selective intracellular electroporation appear somewhat exotic and it is not clear if they exist in living cells [Kotnik and Miklavcic, 2006]. For intracellular effects that occur at levels higher than plasma membrane poration, further analysis is needed to distinguish between direct field effects and secondary physiological effects mediated by the loss of plasma membrane integrity.

With that said, plasma membrane permeabilization may not be the only primary bioeffect of electric pulses. A number of studies by Chen and co-authors indicated that electric pulses of supra-physiological voltage could cause damage to voltage-gated (VG) ion channels [Chen and Lee, 1994a, b; Chen et al., 1998, 2006; Chen, 2004, 2005]. The authors used a modified double Vaseline-gap voltage clamp technique to apply electroporative shocks and measure transmembrane currents in a skeletal muscle fiber. Using 4 ms pulses, the authors reported that increasing the transmembrane potential to 400 mV caused electroporation with no effect on ion channels. However, increasing the pulse amplitude to 600–800 mV caused inhibition of both potassium and sodium voltage-gated channels. The authors explained this effect by electroconformational changes or conformational damage to the proteins that form the VG channels. However, in our opinion, other explanations of the inhibitory effect have not been adequately explored and ruled out (including changed transmembrane ion gradient due to electroporation; reduced efficiency of voltage clamping due to decreased membrane resistance; voltage dependence of leak currents that could affect accurate measurements of VG currents; entry of Ca^{2+} and regulatory modulation of Na^+ and K^+ channels; and general “rundown” of the fiber preparation due to the electroporative membrane disruption; etc.). So far, the findings of inhibition of VG channels by conventional electroporation have not been replicated by other groups or by using other methods.

Compared to ms duration pulses, the use of nsPEF provides an opportunity to reach higher induced membrane potentials without any appreciable thermal effect. Therefore, one may expect that voltage-gated channels may be more vulnerable to nsPEF than to fields of longer pulses. This paper is the first systematic analysis of nsPEF effects on voltage-gated Ca^{2+} and Na^+ channels (I_{Ca} and I_{Na} , respectively), with special emphasis on their relation to membrane permeabilization.

MATERIALS AND METHODS

Cell lines

A murine pituitary cell line (GH3) and a murine neuroblastoma-rat glioma hybrid (NG108) cell line were obtained from American Type Culture Collection (Manassas, VA) and propagated at 37 °C with 5% CO₂ according to the supplier's recommendations. GH3 cells were cultured in Ham's F12K medium supplemented with 2.5% fetal bovine serum (FBS) and 15% horse serum (Atlanta Biologicals, Norcross, GA). NG108 cells were cultured in Dulbecco's Modified Eagle's Medium without sodium pyruvate, supplemented with 4 mM L-glutamine, 4.5 g/L glucose, 10% FBS, 0.2 mM hypoxanthine, 400 nM aminopterin, and 0.016 mM thymidine. The growth media also contained 1% penicillin/streptomycin. The media and its components were obtained from either Mediatech Cellgro (Herndon, VA) or Invitrogen (Eugene, OR). For the passage immediately preceding experiments, cells were transferred onto glass cover slips pre-treated with poly-L-lysine (Sigma-Aldrich, St. Louis, MO).

Electrophysiology

Patch-clamp recording techniques were similar to those described previously [Pakhomov et al., 2007a, 2009; Ibey et al., 2009, 2010]. Recording pipettes were manufactured from borosilicate glass (1B150F-4, World Precision Instruments, Sarasota, FL, or BF150-86-10, Sutter Instrument, Novato, CA). They were pulled to a tip resistance of 1.5-3 MΩ using a Flaming/Brown P-97 micropipette puller (Sutter Instrument). Cells on a cover slip were transferred into a glass-bottomed chamber (Warner Instruments, Hamden, CT) mounted on an IX71 inverted microscope (Olympus America, Center Valley, PA).

I_{Ca} was measured in GH3 cells as a peak inward current carried by Ba²⁺ (10 mM) in response to 200 ms steps from the holding potential of -80 mV to different test potentials (from -70 to +70 mV, with 10 mV increments). Whole-cell currents were measured using a Multiclamp 700B amplifier, Digidata 1322A digitizer, and pCLAMP 10 software (Molecular Devices, Foster City, CA). The analog signal was low-pass filtered at 2 or 5 kHz, and digitized at oversampling rates of 10 to 50 kHz. The series resistance was not compensated.

The extracellular buffer contained (in mM): 136 tetraethylammonium chloride (TEA-Cl), 2 MgCl₂, 10 BaCl₂, 10 N-2-hydroxyethylpiperazine-N'-2-ethanesulfonic acid (HEPES), and 10 glucose (pH 7.4). The pipette solution had (in mM): 20 TEA-Cl, 120 CsCl, 10 Cs-ethylene glycol tetraacetic acid (EGTA), 1 BaCl₂, 10 HEPES, and 4 Mg-ATP (pH 7.2).

I_{Na} was measured in NG108 cells using a similar setup, but with an Axopatch 200B amplifier and Digidata 1440A digitizer (Molecular Devices). The command voltage was stepped from the holding level of -80 mV to test voltages between -100 mV and +30 mV, with 10 mV increments. Shifting the membrane potential to more positive values had to be avoided because it often caused membrane destabilization and abruptly increased leak conductance in nsPEF-treated cells [Pakhomov et al., 2009; Pakhomov and Pakhomova, 2010]. The series resistance was compensated to 60-80%. I_{Na} was measured as a negative peak of the fast-inactivating current within 2-3 ms after the step; the stimulus artifact was subtracted off-line when necessary. The bath buffer was composed of (in mM): 134 NaCl, 10 TEA-Cl, 4 MgCl₂, 1 Na-EGTA, 10 HEPES, and 5 glucose (pH 7.4). The recording pipette was filled with (in mM): 139 CsCl, 1 NaCl, 3 MgCl₂, 5 Cs-EGTA, 10 HEPES, and 1 Mg-ATP (pH 7.2).

The membrane voltages reported in this paper have not been corrected for the junction potential (8.5 mV for I_{Ca} and 5.3 mV for I_{Na}). The osmolality of all solutions was between

290 and 310 mOsm/kg as measured with a freezing point micro-osmometer (Advanced Instruments, Norwood, MA). Chemicals were purchased from Sigma-Aldrich.

Voltage-gated currents were processed with and without normalization to the cell capacitance (pA/pF). Both approaches produced similar results.

Exposure to nsPEF and local E-field modeling

The system for nsPEF delivery to individual cells under a microscope has been described in detail recently [Bowman et al., 2010; Pakhomova et al., 2011]. In brief, nearly rectangular 300 or 600 ns pulses were generated in a transmission line-type circuit upon timed delivery of a trigger pulse. The nsPEF amplitude was measured across a matched 50 Ω load using a 500 MHz P6139A probe connected to a 5 GHz TDS3052 oscilloscope (Tektronix, Beaverton, OR).

The nsPEF was delivered to a selected cell with a pair of tungsten rod electrodes (80–100 μ m diameter, 120–200 μ m gap). These varied electrode configurations are explained by the fact that the electrodes in use could be accidentally damaged or bent, and would need to be replaced with another pair that was not precisely the same. In addition, the electrodes used in experiments with NG108 cells were tapered to 7–10 μ m over the last 260 μ m of their length. All differences in the electrode geometry were taken into account by separate E-field calculations for each electrode configuration, and the pulse generator voltage was properly adjusted to produce the needed E-field at the cell location. E-field calculations were based on 3D simulations with a finite element Maxwell equations' solver (Amaze 3D, Field Precision, Albuquerque, NM), as described in detail previously [Bowman et al., 2010]. Using a robotic micromanipulator, the electrodes were positioned precisely at 50 μ m above the coverslip surface so that the selected cell was in the middle of the gap between their tips.

All exposures were performed at room temperature (23–24 $^{\circ}$ C), and maximum (adiabatic) heating from nsPEF did not exceed 0.02 $^{\circ}$ C. For sham exposures, all procedures were identical but no pulses were applied. Within each series of experiments, sham exposures and nsPEF treatments were carefully randomized.

Cell imaging

To visualize cell plasma membrane permeabilization by nsPEF, the bath buffer was supplemented with 5 μ M propidium iodide (Pr), a fluorescent dye that does not pass the intact cell membrane. Once the membrane integrity is compromised by nsPEF to open pores large enough for Pr, the dye enters the cell and profoundly increases its emission upon binding to nucleic acids. The dye was excited using a Lambda DG-4 illuminator (Sutter Instrument). The emission signal was recorded with a C9100-02 electron multiplier CCD camera (Hamamatsu, Bridgewater, NJ) and processed with MetaFluor software (Molecular Devices).

RESULTS

NsPEF effects on intact NG108 cells

In this series of experiments, cells were first subjected to nsPEF, and only afterward was the recording pipette brought into contact with the cell membrane to establish a whole-cell current recording configuration. As noted earlier, exposure of intact cells is the only true artifact-free approach that poses no concerns if nsPEF effects are caused by the presence of the recording pipette or result from gigaohmic seal damage by nsPEF [Pakhomov et al., 2007a]. However, the drawbacks of this protocol are the inevitable delay between the exposure and the first data recording (120 s on average), and the lack of pre-exposure data

for each individual cell. Hence, the comparison could only be performed between populations of sham-exposed and nsPEF-exposed cells.

Typical currents elicited by voltage steps in sham-exposed and nsPEF-exposed NG108 cells are presented in Figure 1A. I_{Na} is manifested by a fast (<2–3 ms), high amplitude, negative deflection followed by a non-inactivating “leak” current (I_{leak}). In control cells, I_{leak} is negligible (<10–20 pA) but it can be increased profoundly by nsPEF (to 100s of pA). On many occasions, I_{leak} showed an enhancement at negative voltages and inward rectifications, which are characteristic signs of nanoelectropore formation [Pakhomov et al., 2009; Pakhomov and Pakhomova, 2010]. In fact, the early negative peak of the current is the superposition of fast-inactivating I_{Na} and non-inactivating I_{leak} . While the contribution of I_{leak} is negligible in control cells, it becomes significant in nsPEF-treated cells. Hence, “pure” I_{Na} had to be isolated by subtracting “pure” I_{leak} (as measured late in each trace) from the negative peak of the combined current ($I_{Na} + I_{leak}$) measured in the beginning of each trace. A more detailed explanation of this procedure and the respective current-voltage (I-V) curves are provided in Figure 1B.

Figure 2A presents the I-V curves for I_{Na} measured in sham- and nsPEF-exposed cells about 2 min after treatment. A single 300 ns pulse caused more than a 2-fold reduction of I_{Na} at 3 kV/cm ($p < 0.01$, Student’s t-test) and weaker changes at 1.8 kV/cm. Consistent with earlier observations [Pakhomov et al., 2007b; Ibey et al., 2010; Pakhomov and Pakhomova, 2010], the exposure also increased I_{leak} (Fig. 1B).

When the exposed cells were allowed to recover longer and the whole-cell configuration was formed 30–60 s prior to the scheduled data collection at 5, 10, or 15 min after exposure, I_{leak} showed a faster recovery than I_{Na} . At 5 min after exposure, I_{leak} had already decreased about 3-fold (see I_{leak} in Fig 2B,C), although it still did not reach the control level. However, at 5 min after the exposure, I_{Na} remained as low as it was at 2 min and only showed a modest recovery at 15 min. Notably, even holding sham-exposed cells in the bath buffer for 30 min had no inhibitory effect on I_{Na} and did not increase I_{leak} .

nsPEF effects on intact GH3 cells

GH3 cells express L- and T-type calcium channels [Suarez-Kurtz and Kaczorowski, 1988]. Depolarizing voltage steps from the holding level of –80 mV activate both types of Ca^{2+} channels, resulting in a slow inactivating inward current (Fig. 3A). Due to such slow inactivation, I_{Ca} cannot be isolated from I_{leak} by the method described in Figure 1B. Instead, we had to rely on the linear approximation of I_{leak} in the interval from –60 to –90 mV and assume that the linear approximation remains valid for more positive membrane potentials. Hence, for the I-V curves in Figure 3B, I_{Ca} is identified by the non-shaded areas between the extrapolated I_{leak} (dashed line) and the I-V curve.

Notably, I_{leak} induced by nsPEF in GH3 cells was much weaker than in NG108 cells and showed only slight (if any) inward rectification. This difference is readily explained by the ion selectivity of nanoelectropores and the composition of buffers used for these experiments. The nanopores were found to be selectively permeable to small cations, whereas the larger TEA cation (the principal cation of the bath buffer) and Cl^- anion both had poor nanopore permeability [Pakhomov and Pakhomova, 2010]. Hence, the lack of ions that could efficiently carry charges through nanoelectropores explains the modest I_{leak} increase in response to nsPEF. Thanks to the relatively small and almost linear increase of I_{leak} by nsPEF, the method of identifying I_{Ca} shown in Figure 3B appeared reliable, although it would not work reliably for I_{Na} .

Intact GH3 cells were exposed to a single 600 ns pulse at 0 (sham), 1.2, 2.4, or 3.6 kV/cm. In one series of experiments, patch-clamp recording was attempted as soon as possible after the exposure and the data were recorded, on average, 2 min after the treatment (Fig. 3B, top graphs). In a separate series, the cells were allowed to recover for about 9 min before the whole-cell recording configuration was formed, and currents were measured at 10 min (Fig. 3B, bottom graphs).

At 2 min after exposure to 2.4 and 3.6 kV/cm (but not 1.2 kV/cm), nsPEF caused a significant inhibition of I_{Ca} . The leak conductance (measured as a slope of the best fit line) was not affected by 1.2 kV/cm (0.48 ns vs. 0.56 ns in the sham-treated group), but increased to 0.78 and 1.04 ns at 2.4 and 3.6 kV/cm, respectively. Although these data point to a connection between I_{leak} increase and I_{Ca} inhibition, this connection was not necessarily supported by the 10 min measurements. At 10 min, the leak conductance was essentially the same in all the groups (0.31–0.36 ns), but I_{Ca} remained strongly inhibited after 3.6 kV/cm exposure (Fig. 2B).

nsPEF-induced changes in membrane currents in individual cells

Forming the patch-clamp recording configuration prior to nsPEF exposure is the only method to compare pre- and post-exposure currents, and measure currents early after exposure. Although this method may be prone to the artifact of gigaseal damage by nsPEF, we showed earlier that nsPEF-triggered entry of Pr occurred at a distance from the pipette and not at the gigaseal [Pakhomov et al., 2009]. Using a potentiometric fluorescent dye, we have also demonstrated that the command voltage from the recording pipette efficiently controls the membrane potential in nanoporated cells [Pakhomov and Pakhomova, 2010]. These data demonstrate the general possibility of whole-cell data recording in cells that were “patched” prior to nsPEF treatment.

We also confirmed that the gigaohmic seal can survive nsPEF exposure in NG108 cells bathed in the extracellular solution for I_{Na} studies. In a representative experiment, shown in Figure 4, currents were measured at selected time intervals before and after the delivery of a single 300 ns pulse at 4 kV/cm, and cell images (overlapped Pr fluorescence and bright field in order to visualize the pipette and cell borders) were taken every 1 s throughout the experiment. At 20 s after the pulse, I_{leak} markedly increased; the lack of concurrent Pr uptake and the distinctive I–V curve of I_{leak} (inward rectification and higher conductance at most negative potentials) were characteristic of nanopore formation [Pakhomov and Pakhomova, 2010]. Gradual resealing of nanopores was seen at 30 and 120 s, but eventually failed (in the whole-cell configuration, cells are dialyzed with the pipette solution and have limited potential for recovery). Pr had entered the cell from the electroporated anodic pole (far from the pipette and gigaseal), and I_{leak} profoundly increased and became almost linear.

The nanopore formation by itself (20 and 30 s after the pulse) had no immediate effect on I_{Na} . Moreover, I_{Na} just started to decrease at 120 s, when nanopores partially resealed. It decreased further at 300 s, when larger, Pr-permeable pores had opened. However, it is not possible to discern if the reduction in I_{Na} at 300 s was a continuation of the inhibitory process that began earlier, or if it resulted from the opening of the Pr-permeable pores.

For Figure 5, the I–V data for each cell at 20 s prior to exposure were subtracted from the I–V data for the same cell at 20 s after exposure. Hence, the graphs in Figure 5 show changes in I_{Na} and I_{leak} solely because of the cell rundown (sham exposure) and its combination with nsPEF (other groups). The graphs also show no effect of one 300 ns pulse at 1.2 kV/cm, high data variability at 1.5 kV/cm (some cells responded to nsPEF and others did not), and a significant effect at 1.8 kV/cm (although several cells still did not respond). The mean magnitude of I_{Na} reduction by 1.8 kV/cm nsPEF (about 6 pA/pF) was remarkably similar to

the value recorded in intact cells (Fig. 2A), thereby adding confidence that the presence of the recording pipette did not cause artifacts.

The connection between I_{leak} increase and I_{Na} inhibition

In Figure 6, the peak amplitude of I_{Na} in 82 individual cells at 20 s post exposure is expressed as a percentage of the pre-exposure value, and plotted against the respective I_{leak} in the same individual cell. This combined plot includes data from several different experimental series that were performed over a 1.5-year period.

The data show that increasing the I_{leak} up to 250 pA (as measured at -90 mV) was not accompanied by a suppression of I_{Na} (mean values of I_{Na} were $98.6 \pm 1.3\%$ in sham-exposed controls and $97.9 \pm 1.2\%$ in nsPEF-treated cells). A further increase in I_{leak} was clearly associated with the inhibition of I_{Na} , although with a high degree of variability; the correlation coefficient was only -0.72 .

The lack of a strict dependence of I_{Na} on I_{leak} is further illustrated in Figure 7. In three individual cells (A–C), nsPEF caused permeabilization of the plasma membrane manifested by a reversible (A and B) or apparently irreversible (C) increase in I_{leak} . The I–V curves in A and B showed inward rectification typical of nanopore formation; I_{leak} in Figure 7C had much higher amplitude and the curve was almost linear, indicating formation of larger “conventional” electropores. Concurrent I_{Na} showed no fluctuations or just minor changes, which also did not coincide with maximum I_{leak} .

DISCUSSION

This study has demonstrated two principal effects of nsPEF, namely permeabilization of the cell plasma membrane and inhibition of voltage-gated I_{Na} and I_{Ca} .

Membrane permeabilization was manifested by an abrupt and profound increase of I_{leak} (by one to two orders of magnitude). In many cells, the nsPEF-induced leak conductance increased at high negative membrane potentials and showed inward rectification, which have been regarded as signs of nanopore formation [Pakhomov et al., 2009, 2010; Ibey et al., 2010]. In cells that were not patched, nanopores resealed and I_{leak} diminished 5–15 min after exposure, which is consistent with earlier data [Pakhomov et al., 2007a]. On several occasions, nanopore resealing was observed even in cells dialyzed with the pipette solution, e.g., in Figure 7A,B. Notably, the lack of nanopore-permeable cations in the bath buffer used for I_{Ca} experiments in GH3 cells resulted in a much weaker I_{leak} increase, simply because there was no charge carrier for the inward current. When tested with different bath buffers, GH3 cells showed the same sensitivity to permeabilization by nsPEF as NG108 cells [Bowman et al., 2010].

When a membrane current is determined by both active (voltage-dependent) and passive (voltage-independent) membrane conductances, the former can be separated using a so-called P/N subtraction method [Molleman, 2002]. This method relies on measurements of the passive current elicited by small voltage steps, and assumes that larger steps induce proportionally larger passive currents. The P/N subtraction was used by Chen and co-authors throughout their studies, and no raw data (before P/N subtraction) were presented [Chen and Lee, 1994a, b; Chen et al., 1998, 2006; Chen, 2004, 2005]. P/N subtraction was not used in our experiments because it would yield highly erroneous data because of the non-linear voltage dependence of I_{leak} (e.g., see Figs. 1, 2, 4, 5, 7). Chen and co-authors did not report if the leak conductance under their experimental conditions was voltage-independent; therefore, it remains uncertain if the P/N subtraction produced accurate measurements of VG

currents. They also did not report the value of the leak conductance at the time when the VG currents were measured.

Despite these uncertainties, our experiments agree with those of Chen et al. – that the inhibition of VG currents only occurred at the E-field levels higher than the threshold for membrane electroporation. Hence, we could observe marked increases in I_{leak} with no simultaneous change in the VG currents. On the other hand, the VG currents could remain inhibited at later time points after exposure, when the I_{leak} had already recovered. These two observations make it clear that the correlation between the increase in I_{leak} and the inhibition of the VG currents is weak. Most importantly, these observations also prove that the decreases in I_{Na} and I_{Ca} were not an artifact from improper operation of the patch-clamp system or inaccurate measurement of the currents in electroporated cells. This conclusion is not as trivial as it may appear, as the accuracy of recording whole-cell currents is critically dependent on a high enough resistance of the cell membrane and the integrity of the seal between the membrane and the recording pipette [Molleman, 2002].

Although the inhibition of I_{Na} and I_{Ca} could start later and outlast the nsPEF-induced increase in I_{leak} , it remains to be studied if the increased I_{leak} was the cause of the inhibition. The conclusion of Chen et al. about electroconformational damage to ion channel proteins appears premature because such damage has not been incontrovertibly demonstrated, and because other mechanisms have not been ruled out. The most trivial explanation would be the reduction of the transmembrane ion gradient due to I_{leak} ; for example, a decreased Na^+ gradient across the membrane will reduce the amplitude of I_{Na} . Although the intracellular Na^+ concentration is strongly buffered by the large volume of the pipette solution, the efficiency of this buffering in comparison with Na^+ leak into the cell through electropores is difficult to estimate, and also depends on the magnitude of I_{leak} . The same considerations apply to the Vaseline-gap method used by Chen et al.

One can also speculate that the inhibition of VG currents is an active regulatory response of the cell. VG channels are regulated by multiple pathways and depend on intracellular ions, particularly Ca^{2+} [Catterall, 2000, 2010; Hille, 2001]. It would come as no surprise if the disruption of the plasma membrane by electroporation affects these pathways and the level of internal Ca^{2+} . Although the latter was buffered by EGTA, the use of a high concentration of a faster Ca^{2+} chelator such as 1,2-bis(o-aminophenoxy)ethane-N,N,N',N'-tetraacetic acid (BAPTA) is a prerequisite to rule out Ca^{2+} -dependent responses.

At present, the weak correlation between I_{leak} and the inhibition of I_{Na} and I_{Ca} , the delayed recovery of I_{Na} and I_{Ca} compared to I_{leak} , and the modest increase in I_{leak} that accompanied the inhibition of I_{Ca} are indirect signs that I_{leak} is not necessarily the primary cause of the inhibition of the VG channels. However, it will take much more research to prove that this inhibition is indeed a separate phenomenon. In particular, it will be interesting to see if moving to still shorter electric pulses (e.g., 1–60 ns) and applying higher E-fields could inhibit VG channels in the absence of any appreciable membrane permeabilization.

Acknowledgments

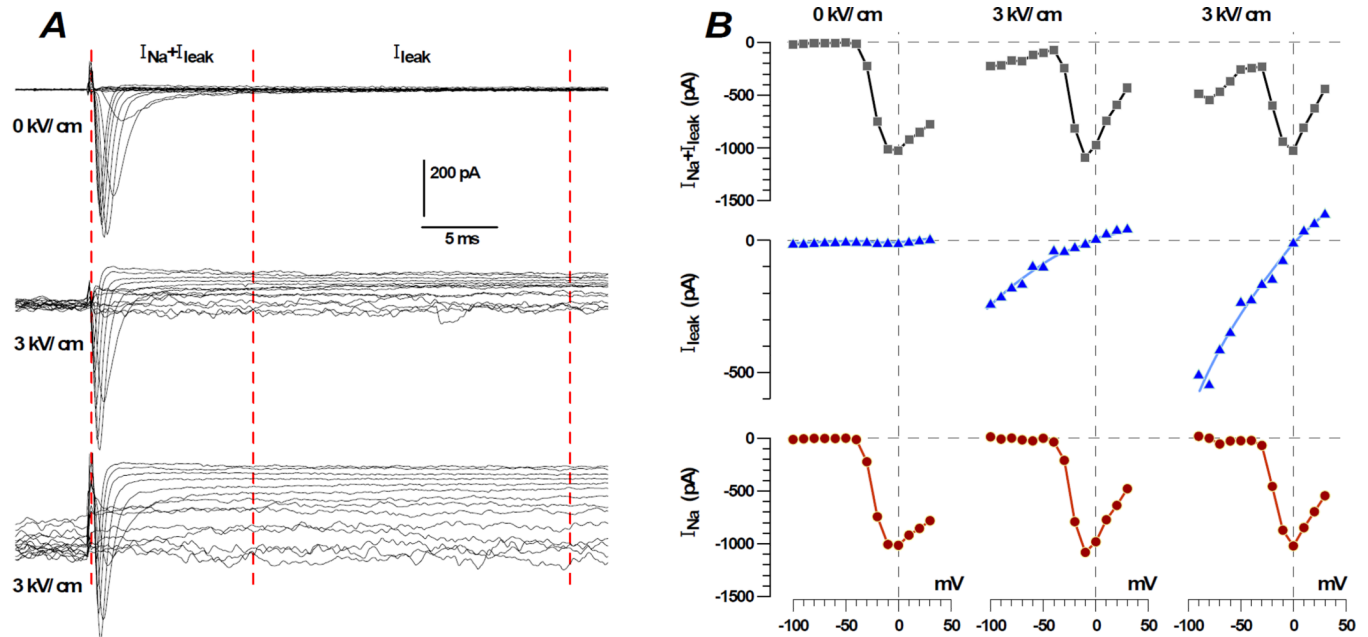
Grant Sponsors: National Cancer Institute, Grant number: R01CA125482; National Institute of General Medical Sciences, Grant number: R01GM088303; Air Force Office of Scientific Research, Grant number: LRIR 09RH09COR.

References

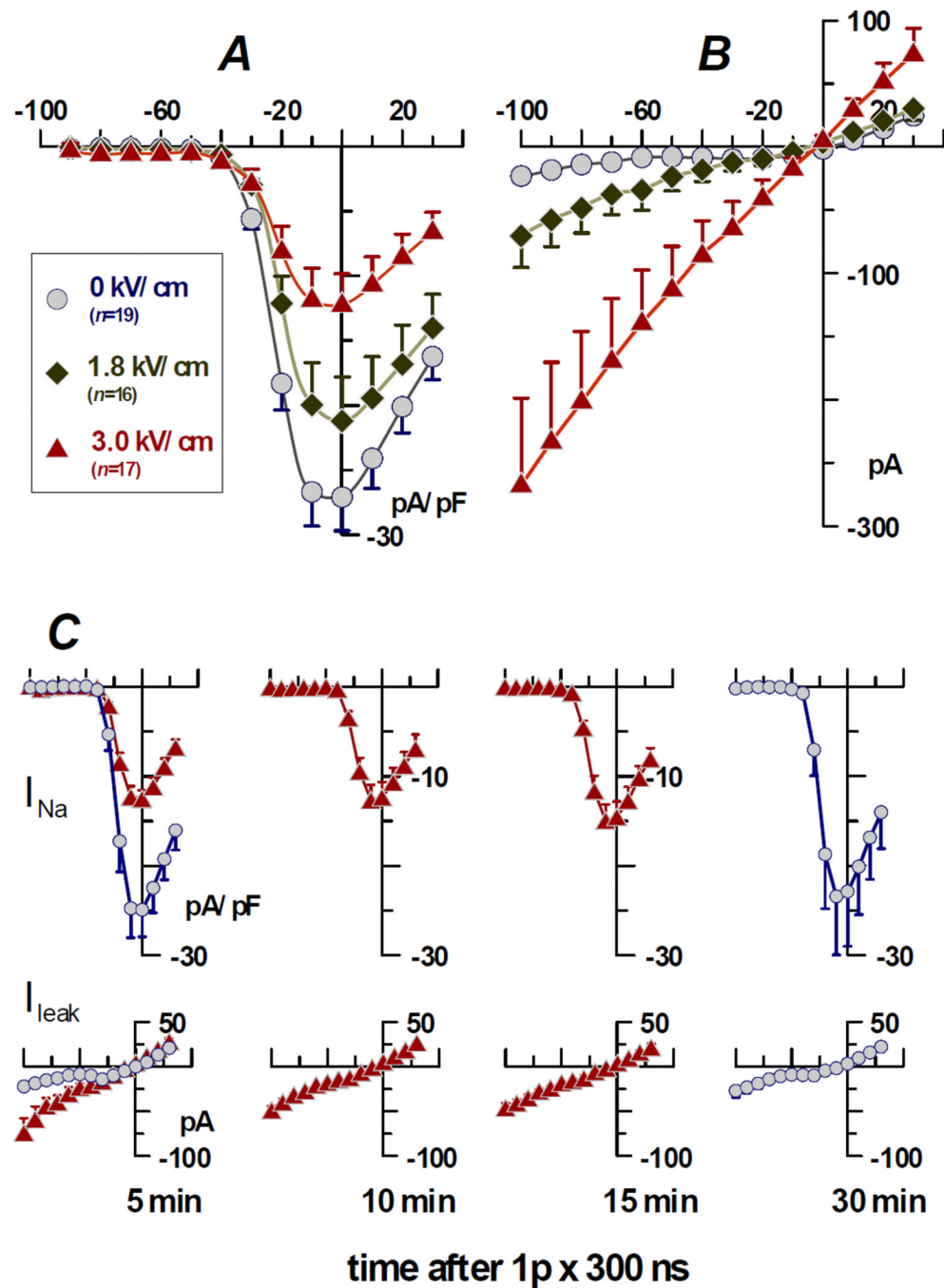
Beebe SJ, Fox PM, Rec LJ, Willis EL, Schoenbach KH. Nanosecond, high-intensity pulsed electric fields induce apoptosis in human cells. *FASEB J*. 2003a; 17:1493–1495. [PubMed: 12824299]

- Beebe SJ, White J, Blackmore PF, Deng Y, Somers K, Schoenbach KH. Diverse effects of nanosecond pulsed electric fields on cells and tissues. *DNA Cell Biol.* 2003b; 22:785–796. [PubMed: 14683589]
- Bowman AM, Nesin OM, Pakhomova ON, Pakhomov AG. Analysis of plasma membrane integrity by fluorescent detection of Ti^+ uptake. *J Membr Biol.* 2010; 236:15–26. [PubMed: 20623351]
- Catterall WA. Structure and regulation of voltage-gated Ca^{2+} channels. *Annu Rev Cell Dev Biol.* 2000; 16:521–555. [PubMed: 11031246]
- Catterall WA. Signaling complexes of voltage-gated sodium and calcium channels. *Neurosci Lett.* 2010; 486:107–116. [PubMed: 20816922]
- Chen W. Supra-physiological membrane potential induced conformational changes in K^+ channel conducting system of skeletal muscle fibers. *Bioelectrochemistry.* 2004; 62:47–56. [PubMed: 14990325]
- Chen W. Electroconformational denaturation of membrane proteins. *Ann N Y Acad Sci.* 2005; 1066:92–105. [PubMed: 16533921]
- Chen W, Han Y, Chen Y, Astumian D. Electric field-induced functional reductions in the K^+ channels mainly resulted from supramembrane potential-mediated electroconformational changes. *Biophys J.* 1998; 75:196–206. [PubMed: 9649379]
- Chen W, Lee RC. Altered ion channel conductance and ionic selectivity induced by large imposed membrane potential pulse. *Biophys J.* 1994a; 67:603–612. [PubMed: 7948676]
- Chen W, Lee RC. Evidence for electrical shock-induced conformational damage of voltage-gated ionic channels. *Ann N Y Acad Sci.* 1994b; 720:124–135. [PubMed: 8010631]
- Chen W, Zhongsheng Z, Lee RC. Supramembrane potential-induced electroconformational changes in sodium channel proteins: A potential mechanism involved in electric injury. *Burns.* 2006; 32:52–59. [PubMed: 16384650]
- Deng J, Schoenbach KH, Buescher ES, Hair PS, Fox PM, Beebe SJ. The effects of intense submicrosecond electrical pulses on cells. *Biophys J.* 2003; 84:2709–2714. [PubMed: 12668479]
- Hille, B. *Ionic Channels of Excitable Membranes.* Sunderland, MA: Sinauer Associates; 2001.
- Ibey BL, Mixon DG, Payne JA, Bowman A, Sickendick K, Wilmlink GJ, Roach WP, Pakhomov AG. Plasma membrane permeabilization by trains of ultrashort electric pulses. *Bioelectrochemistry.* 2010; 79:114–121. [PubMed: 20171148]
- Ibey BL, Xiao S, Schoenbach KH, Murphy MR, Pakhomov AG. Plasma membrane permeabilization by 60- and 600-ns electric pulses is determined by the absorbed dose. *Bioelectromagnetics.* 2009; 30:92–99. [PubMed: 18839412]
- Kotnik T, Miklavcic D. Theoretical evaluation of voltage inducement on internal membranes of biological cells exposed to electric fields. *Biophys J.* 2006; 90:480–491. [PubMed: 16239325]
- Mollemann, A. *Patch Clamping: An Introductory Guide to Patch Clamp Electrophysiology.* Padstow, Cornwall, Great Britain: John Wiley and Sons; 2002.
- Napotnik TB, Rebersek M, Kotnik T, Lebrasseur E, Cabodevila G, Miklavcic D. Electroporation of endocytotic vesicles in B16 F1 mouse melanoma cells. *Med Biol Eng Comput.* 2010; 48:407–413. [PubMed: 20361267]
- Neumann, E.; Sowers, AE.; Jordan, CA., editors. *Electroporation and Electrofusion in Cell Biology.* New York: Plenum; 1989.
- Pakhomov AG, Kolb JF, White JA, Joshi RP, Xiao S, Schoenbach KH. Long-lasting plasma membrane permeabilization in mammalian cells by nanosecond pulsed electric field (nsPEF). *Bioelectromagnetics.* 2007a; 28:655–663. [PubMed: 17654532]
- Pakhomov AG, Shevin R, White JA, Kolb JF, Pakhomova ON, Joshi RP, Schoenbach KH. Membrane permeabilization and cell damage by ultrashort electric field shocks. *Arch Biochem Biophys.* 2007b; 465:109–118. [PubMed: 17555703]
- Pakhomov AG, Bowman AM, Ibey BL, Andre FM, Pakhomova ON, Schoenbach KH. Lipid nanopores can form a stable, ion channel-like conduction pathway in cell membrane. *Biochem Biophys Res Commun.* 2009; 385:181–186. [PubMed: 19450553]
- Pakhomov, AG.; Miklavcic, D.; Markov, MS., editors. *Advanced Electroporation Techniques in Biology in Medicine.* Boca Raton, FL: CRC Press; 2010. 528 p.

- Pakhomov, AG.; Pakhomova, ON. Nanopores: A distinct transmembrane passageway in electroporated cells. In: Pakhomov, AG.; Miklavcic, D.; Markov, MS., editors. *Advanced Electroporation Techniques in Biology in Medicine*. Boca Raton, FL: CRC Press; 2010. p. 178-194.
- Pakhomova ON, Gregory BW, Khorokhorina VA, Bowman AM, Xiao S, Pakhomov AG. Electroporation-induced electrosensitization. *PLoS One*. 2011; 6:e17100. [PubMed: 21347394]
- Ren W, Beebe SJ. An apoptosis targeted stimulus with nanosecond pulsed electric fields (nsPEFs) in E4 squamous cell carcinoma. *Apoptosis*. 2011; 16:382–393. [PubMed: 21213047]
- Rubinsky, B. *Irreversible Electroporation*. Berlin, Heidelberg: Springer-Verlag; 2010.
- Schoenbach KH, Beebe SJ, Buescher ES. Intracellular effect of ultrashort electrical pulses. *Bioelectromagnetics*. 2001; 22:440–448. [PubMed: 11536285]
- Schoenbach KS, Hargrave B, Joshi RP, Kolb J, Osgood C, Nuccitelli R, Pakhomov AG, Swanson J, Stacey M, White JA, Xiao S, Zhang J. Bioelectric effects of nanosecond pulses. *IEEE Transactions on Dielectrics and Electrical Insulation*. 2007; 14:1088–1109.
- Suarez-Kurtz G, Kaczorowski GJ. Effects of dichlorobenzamil on calcium currents in clonal GH3 pituitary cells. *J Pharmacol Exp Ther*. 1988; 247:248–253. [PubMed: 2845054]
- Teissie J, Eynard N, Gabriel B, Rols MP. Electroporation of cell membranes. *Adv Drug Deliv Rev*. 1999; 35:3–19. [PubMed: 10837686]
- Vernier PT, Sun Y, Gundersen MA. Nanoelectropulse-driven membrane perturbation and small molecule permeabilization. *BMC Cell Biol*. 2006; 7:37. [PubMed: 17052354]
- Vernier PT, Sun Y, Marcu L, Craft CM, Gundersen MA. Nanoelectropulse-induced phosphatidylserine translocation. *Biophys J*. 2004; 86:4040–4048. [PubMed: 15189899]
- Weaver JC. Electroporation of cells and tissues. *IEEE Trans Plasma Sci*. 2000; 28:24–33.
- White JA, Blackmore PF, Schoenbach KH, Beebe SJ. Stimulation of capacitative calcium entry in HL-60 cells by nanosecond pulsed electric fields. *J Biol Chem*. 2004; 279:22964–22972. [PubMed: 15026420]
- Zimmermann, U.; Neil, GA. *Electromanipulation of cells*. Boca Raton, FL: CRC Press; 1996.

**Fig. 1.**

Typical membrane currents and measurement of I_{Na} in control and nsPEF-exposed NG108 cells. **A:** Original current traces in three different cells about 120 s after sham (0 kV/cm) or nsPEF exposure (one 300 ns pulse at 3 kV/cm). Note the fast inactivating inward current (I_{Na}) and non-inactivating current (I_{leak}), which is more pronounced in nsPEF-treated cells. **B:** Current-voltage (I-V) curves as measured from traces in panel A. The combined current ($I_{Na} + I_{leak}$) was measured as a negative peak of current traces during the interval immediately following the voltage step. I_{leak} was measured as a mean value of non-inactivating currents approximately 10–40 ms after voltage stepping.

**Fig. 2.**

Effect of E-field amplitude and time interval after exposure (one 300 ns pulse) on I_{Na} and non-inactivating I_{leak} . **A:** I-V curves for I_{Na} measured about 2 min after nsPEF (1.8 and 3 kV/cm) or sham exposure (0 kV/cm). **B:** Respective I_{leak} values in the same cells. **C:** I_{Na} and I_{leak} as measured at indicated time intervals after 3 kV/cm or sham exposure ($n=5-8$ in each group). Note the fast restoration of I_{leak} but not I_{Na} in nsPEF-treated cells. Holding control cells in the bath for 30 min after sham exposure (rightmost panel) had no effect on the currents.

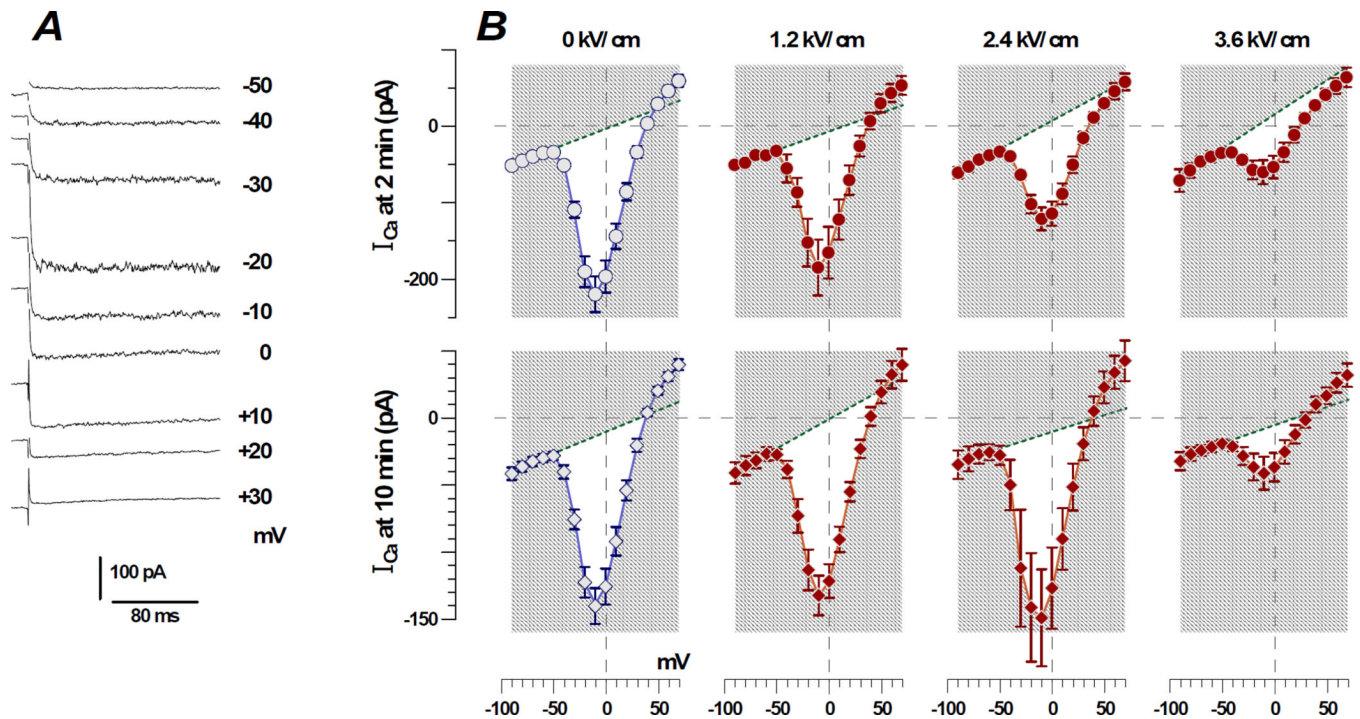


Fig. 3.

Voltage-gated I_{Ca} in GH3 cells and its inhibition by nsPEF. **A:** Traces of the current elicited by stepping the command voltage from the holding potential of -80 mV to various test potentials (as indicated next to the traces). For clarity, the traces are spatially separated and shown below each other. **B:** GH3 cells were exposed intact to one 600 ns pulse at 0, 1.2, 2.4, or 3.6 kV/cm. Whole-cell currents were measured about 2 min (top) or 10 min (bottom) after exposure. In the latter groups, cells were allowed to recover for about 9 min prior to being patched. Each graph shows the mean \pm SE for 8–15 independent experiments; I_{Ca} is identified by the area free of shading.

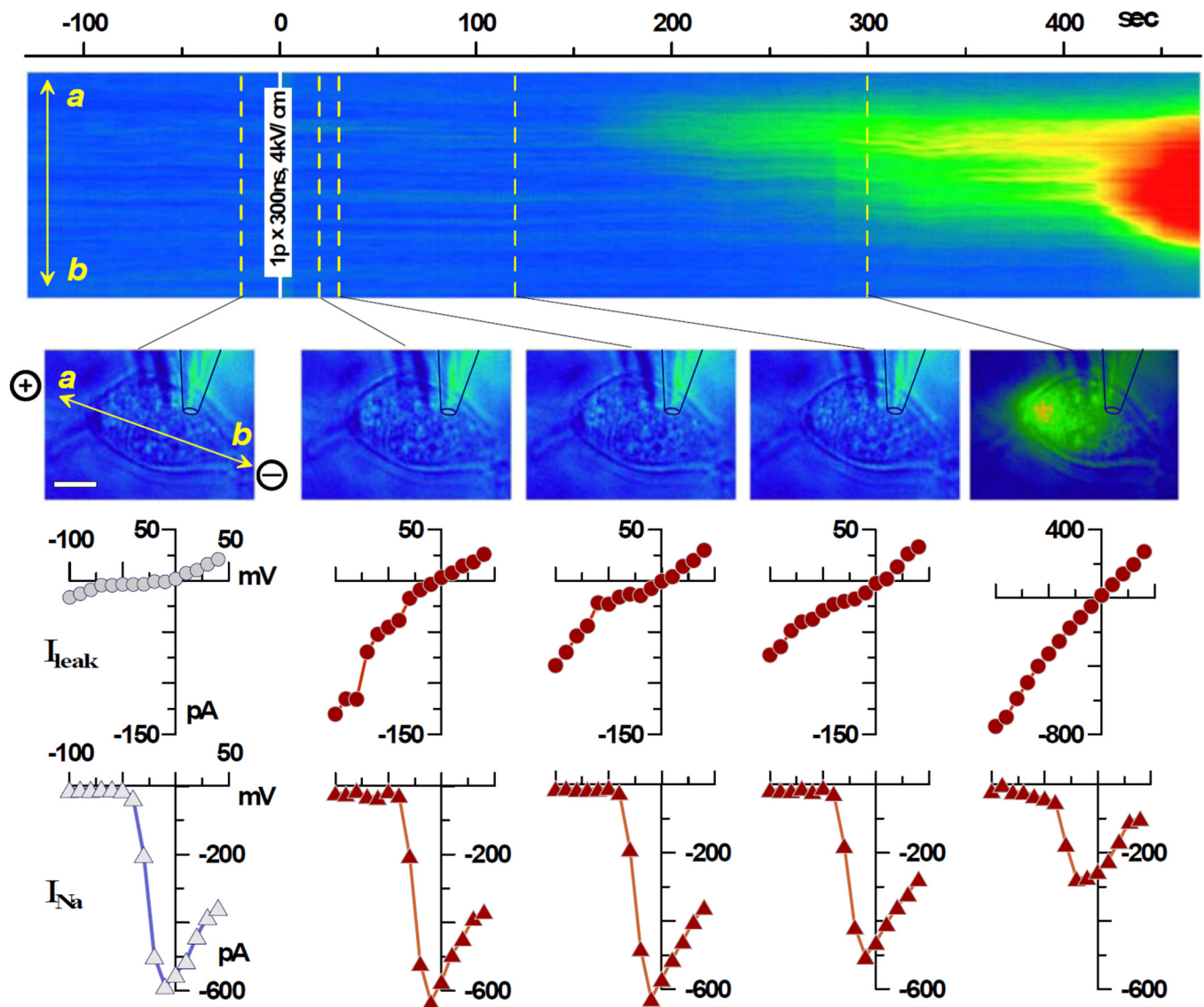


Fig. 4.

Localized propidium iodide uptake and typical membrane currents following nsPEF exposure. Top: Time change display of fluorescence intensity (pseudocolor) along the line *a-b* between nsPEF-delivering electrodes. One 300 ns pulse at 4 kV/cm was delivered at 0 s. Middle: Images of the entire cell fluorescence at selected timepoints (identified by dashed lines on the time change display). The left image also shows the position of the line *a-b* relative to the cell body and recording pipette (outlined for clarity). “+” and “-” signs show directions of nsPEF-delivering electrodes to the anode and cathode. Scale bar: 10 µm. Bottom: I-V curves of I_{leak} and I_{Na} for the same timepoints as the cell images. Note that propidium iodide uptake was delayed after exposure and occurred at the anodic pole of the cell, far from the recording pipette. It was accompanied by profound I_{leak} enhancement (note the different scale for the rightmost graph), loss of inward rectification, and decrease of I_{Na} .

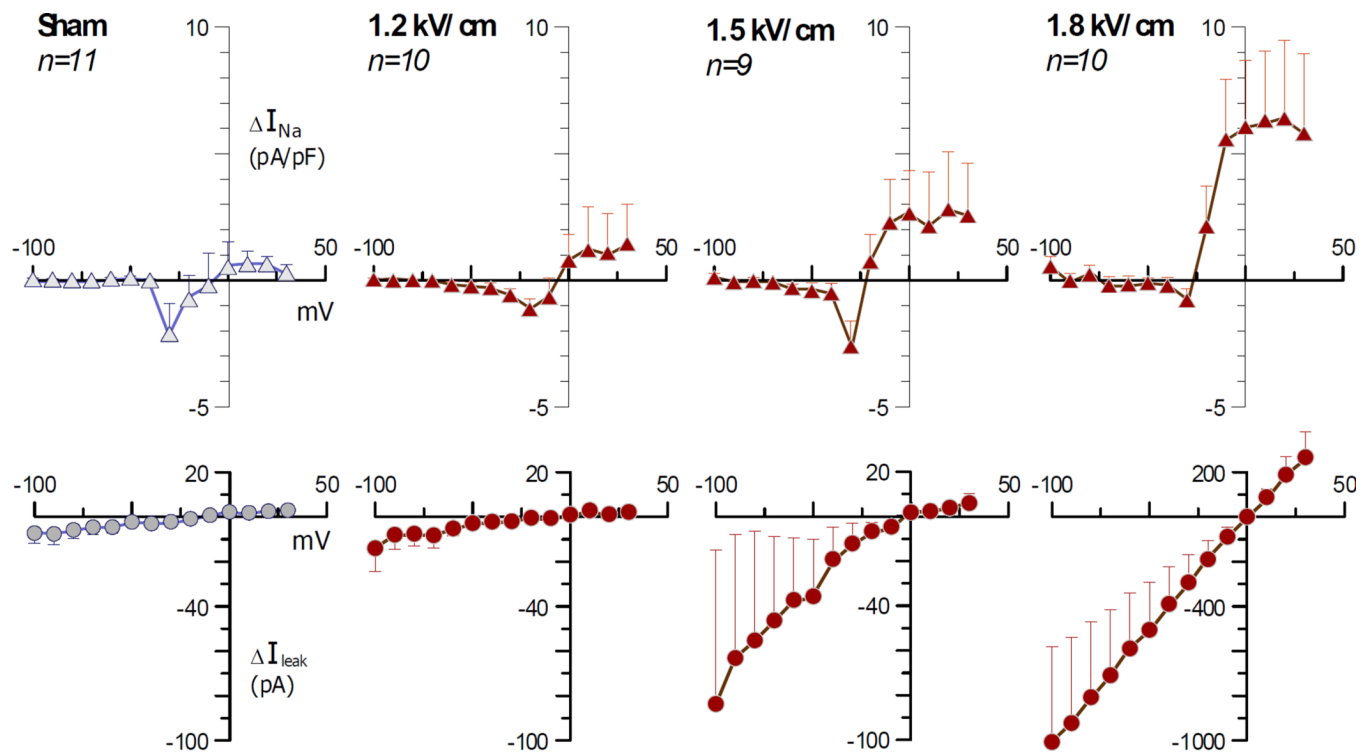


Fig. 5.

Mean changes of I_{Na} and I_{leak} in individual NG108 cells exposed to one 300 ns electric pulse at different E-field intensities. I-V data in each individual cell were collected 20 s prior to and 20 s after nsPEF exposure; the former was then subtracted from the latter. This difference was averaged for all the cells that underwent the same treatment. Note the different vertical scale for I_{leak} after 1.8 kV/cm.

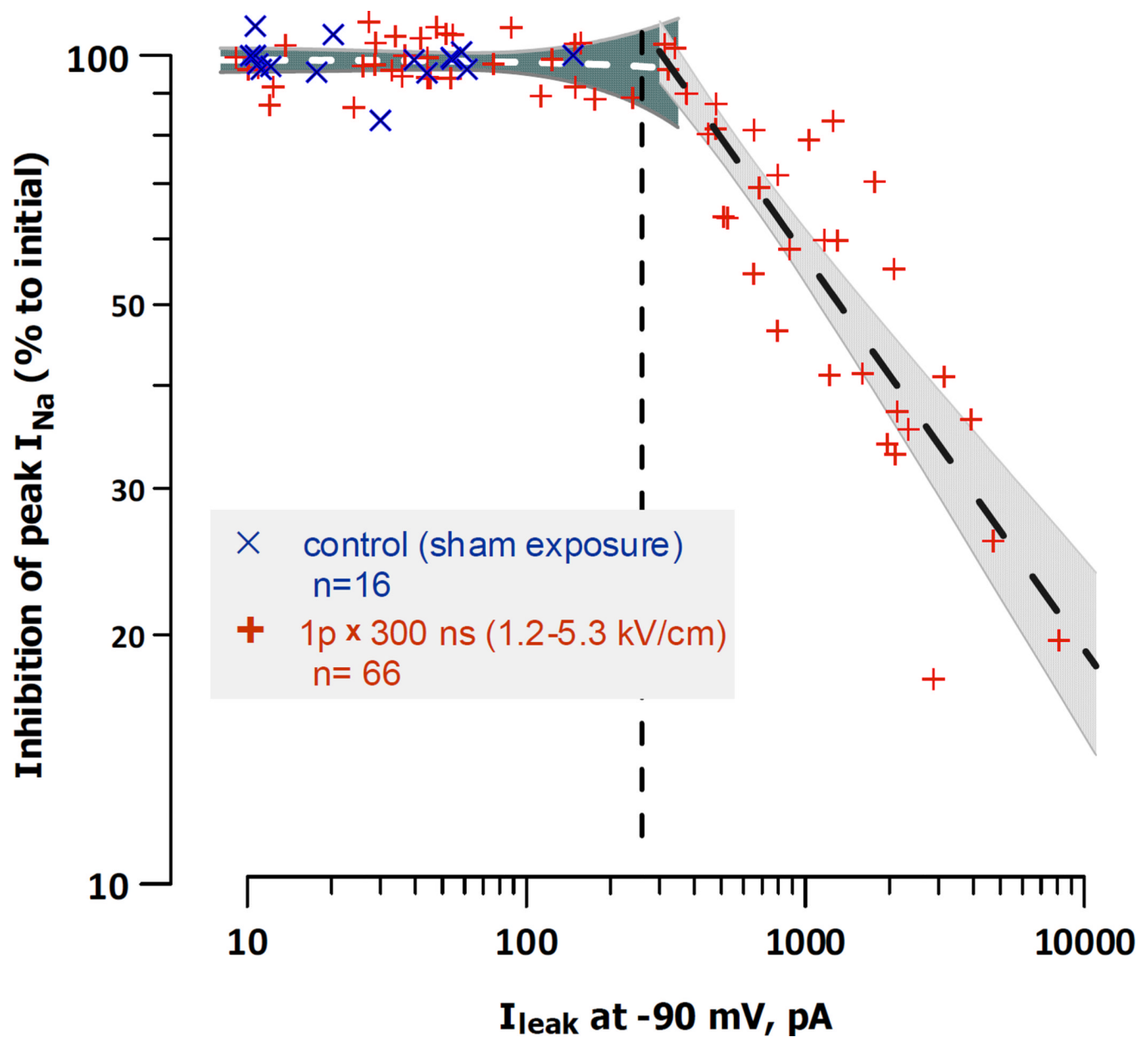


Fig. 6.

Degree of inhibition of I_{Na} as a function of I_{leak} amplitude in individual cells. Currents were measured 10 s after nsPEF exposure, and the maximum amplitude of I_{Na} is expressed as a percentage of its pre-exposure value. Note the lack of inhibition of I_{Na} when nsPEF-induced I_{leak} did not exceed 250 pA. Dashed lines are the best fit power function approximations, separately for $I_{leak} < 250$ pA and $I_{leak} > 250$ pA. Shaded areas are the 95% confidence intervals of the approximations.

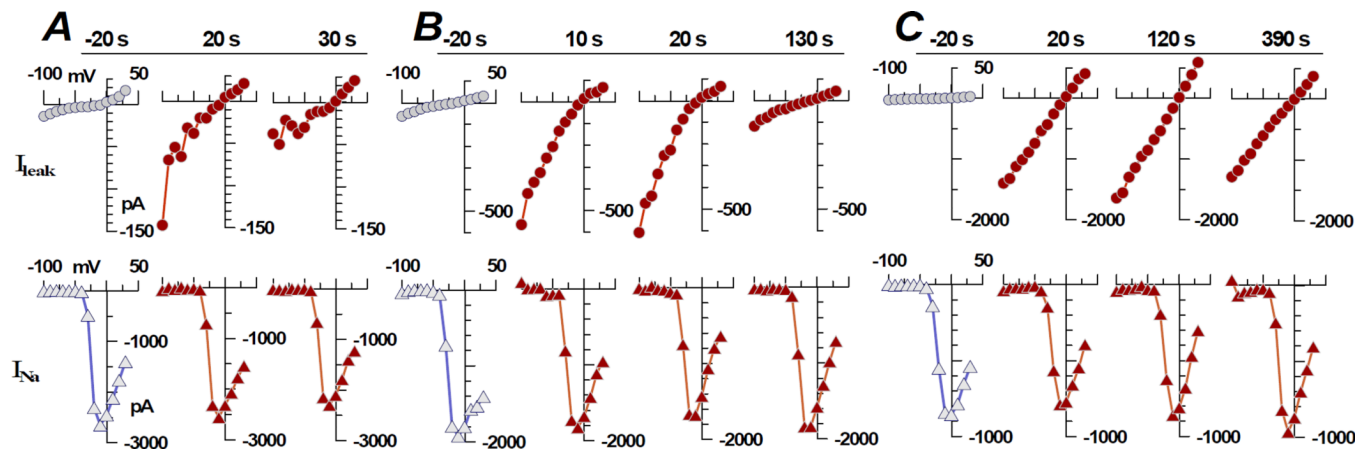


Fig. 7.

Lack of a strict connection between the nsPEF-induced inhibition of voltage-gated I_{Na} and the increase in I_{leak} . **A, B, C:** Three individual experiments on NG108 cells exposed to a single 300 ns pulse at 1.5 (**A** and **B**) or 1.8 kV/cm (**C**) at 0 s. I–V data are shown for a single timepoint prior to nsEP exposure (–20 s, gray symbols) and for indicated times after.